Supporting Information of

Enhancing cycle-life of initial-anode-free lithium-metal battery by pre-lithiation in Mn-based Li-rich spinel cathode

Leiyu Chen,[a]‡ Chao-Lung Chiang,[b]‡ Guifan Zeng,[a] Yonglin Tang,[a] Xiaohong Wu,[a] Shiyuan Zhou,[a] Baodan Zhang,[a] Haitang Zhang,[a] Yawen Yan,[a] Tingting Liu,[d] Hong-Gang Liao,[a] Chuanwei Wang,*[e] Xiaoxiao Kuai,*[ac] Yan-Gu Lin,*[b] Yu Qiao,*[ac] Shi-Gang Sun[a]

[a] State Key Laboratory of Physical Chemistry of Solid Surfaces, iChEM (Collaborative Innovation Center of Chemistry for Energy Materials), Department of Chemistry, College of Chemistry and Chemical Engineering, Xiamen University, Xiamen, 361005, PR China

[b] National Synchrotron Radiation Research Center, Hsinchu 30076 Taiwan, R.O.C.

[c] Fujian Science & Technology Innovation Laboratory for Energy Materials of China (Tan Kah Kee Innovation Laboratory), Xiamen, 361005, PR China

[d] School of Environmental Science and Engineering, Suzhou University of Science and Technology, Suzhou 215009, China

[e] Cell research department, Amperex Technology Limited, Ningde, 352100, China

* Correspondence to: Wangcw2@atlbattery.com (C. W.)

kuaixiaoxiao@xmu.edu.cn (X. K.)

lin.yg@nsrrc.org.tw (Y. G. L.)

yuqiao@xmu.edu.cn (Y. Q.)

‡ L. Chen and C.-L. Chiang contributed equally to this work.

Experimental Section

Preparation of $LiMn_2O_4$(LMO) cathode

Fd-3m type LMO (Adamas-beta, Shanghai Titan Scientific Co.,Ltd) was vacuum dried at 110℃ for 12 h. The LMO cathode black slurry consisted of 80% of the active materials, 10% of the carbon black powder (Super P, Timcal), and 10% of the polyvinylidene fluoride (PVDF, Guangdong Canrd New Energy Technology Co., Ltd.) binder in weight, with N-methyl-2-pyrrolidone (NMP, Guangdong Canrd New Energy Technology Co., Ltd.) solvent, and then the black slurry was stirred in SK-300SII CE mixing machine for 25 min. Then, coating the black slurry onto a clean carbon coated aluminum foil (Suzhou Sinero Technology Co., Ltd.) by a doctor blade. After solvent drying, the loaded foil was roll-pressed and was punched into disk followed by additional vacuum drying at 110 ℃ for 12 h. The typical mass loading of LMO in cathode is about 7 mg cm^{-2} (Li||LMO half-cell) or 8.5 mg cm^{-2} (Cu||LMO anode-free cell) on average, respectively. Then, the LMO cathodes were punched into discs with a diameter of 11 mm.

Preparation of $Li_xMn_2O_4$(L_xMO) cathode

L_xMO ($0 \leq x \leq 2$) cathodes were fabricated by electrochemical pre-lithiation and contact pre-lithiation method. As for the electrochemical pre-lithiation method, the L_xMO cathodes were prepared by over discharge of LMO cathodes in Li||LMO half-cells, since there are sufficient Li resources on the counter electrodes. The x vale can be controlled by the discharge cut-off potential. As for contact pre-lithiation method, the lithium metal foil (China Energy Lithium Co.,

Ltd.) contacted directly with the LMO cathode which saturated with pre-prepared electrolytes, then L_xMO cathodes were obtained with different x vale which can be controlled by contact time.

Preparation of half-cells, anode-free-cells and in-situ cell

Li||LMO half-cells were assembled in CR2032-type coin cells with LMO cathodes as working electrodes, lithium metal foil as counter electrodes, Celgard 2325 (Whatman Co., Ltd.) as separator, and 1 M $LiPF_6$ in ethyl carbonate/ethyl methyl carbonate (EC/EMC) with a ratio of 3:7 in volume as the electrolyte (base electrolyte, Suzhou Duoduo Chemical Technology Co., Ltd). Cu||LMO anode-free cells were assembled using a similar protocol, but using Cu foil (16 mm) as counter electrode, and base electrolyte or 1M $LiPF_6$ and 0.02M LiDFOB in fluoroethylene carbonate/hydrogen fluoride-ether/fluoroethylene methyl carbonate (FEC/HFE/FEMC) with a ratio of 2:2:6 in mass as the electrolyte (fluorine-containing electrolyte, Suzhou Duoduo Chemical Technology Co., Ltd.). The electrolyte addition in each coin-cells was 75 μL The Li||LMO *in-situ* cell was assembled using a similar protocol, but with *in-situ* electrochemical cell.

Characterizations

The X-ray diffraction (XRD) patterns were performed on Rigaku SmartLab-SE Powder X-ray diffractometer fitted with Cu-Kα X-rays (λ = 1.5406Å) radiation at a scan rate of 2 °/min in the scan range (2θ) of 10-80 °. The data of *in-situ* XRD for every single pattern was collected for 10 min with scan rage (2θ) of 15-60 °. The high-resolution transmission electron microscopy (HRTEM) images of LMO were obtained by JEOL JEM-2100 Plus transmission electron

microscope, operated at 200 kV. X-ray absorption spectroscopy (XAS) spectra were collected in transmission mode at beamline 1W1B of the Taiwan Photon Source Beamline (TPS 44A) station of the National Synchrotron Radiation Research Center (NSRRC) in Hsinchu, Taiwan. The different voltage states of LMO samples and standards were analyzed by using X-ray absorption near-edge structure spectra (XANES). After XANES data processed in Athena software, XANES spectra were normalized for further comparisons. The R-space of samples were Fourier-transformed (FT) from these calibrated and normalized extended X-ray absorption fine structure (EXAFS) spectra to further explore the internal structure. To supplement the EXAFS fitting results, wavelet transform (WT) analysis of Mn *K-edge* spectra is further performed to explore more intuitive changes of the surrounding coordination environments of transition metal (TM).

Electrochemical measurements

Galvanostatic cycling tests were conducted within a voltage window of 3.2-4.35 V (Li||LMO half-cells/Cu||LMO anode-free coin cells using Neware battery cycler (CT-4008T-5 V10 mA-164) at 26 °C. All cells were (dis)charged at 0.2C or 0.5C or 1C (1C = 148 mA g^{-1}). A CHI 660d workstation was used to collect the linear sweep voltammetry (LSV) patterns at a scan rate of 0.05 mV s^{-1}.

Supplementary Figures/Table

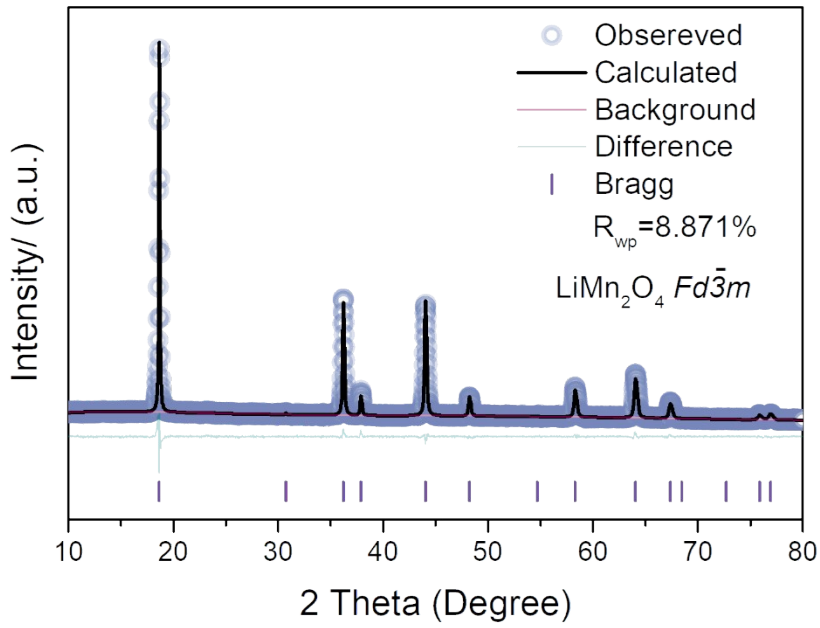

Fig. S1 Representative refinement pattern of *Fd-3m* type $LiMn_2O_4$.

Table S1 Rietveld refinement results on the XRD pattern of *Fd-3m* type $LiMn_2O_4$.

Space group Fd-3m.			R_{wp}=8.871%	Chi2=2.30	
a (Å)	8.2125(6)			α (°)	90
b (Å)	8.2125(6)			β (°)	90
c (Å)	8.2125(6)			γ (°)	90
Atom	Site	x	y	z	Occ
Li	8a	0.12500	0.12500	0.12500	1
Mn	16d	0.50000	0.50000	0.50000	1
O	32e	0.26111	0.26111	0.26111	1

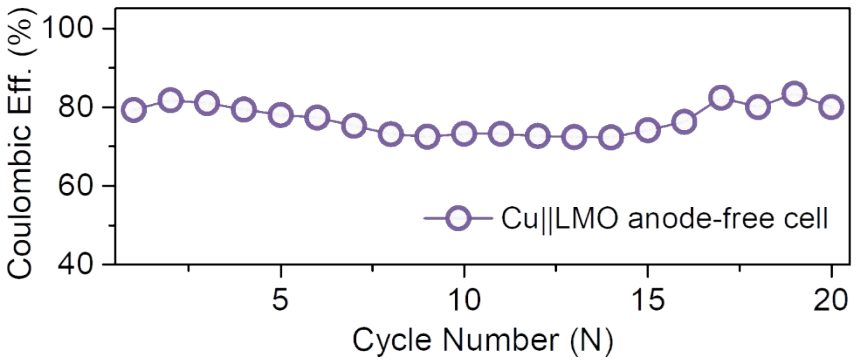

Fig. S2 Coulombic efficiency of Cu||LMO anode-free cell under a voltage window of 3.2-4.35 V at 3C.

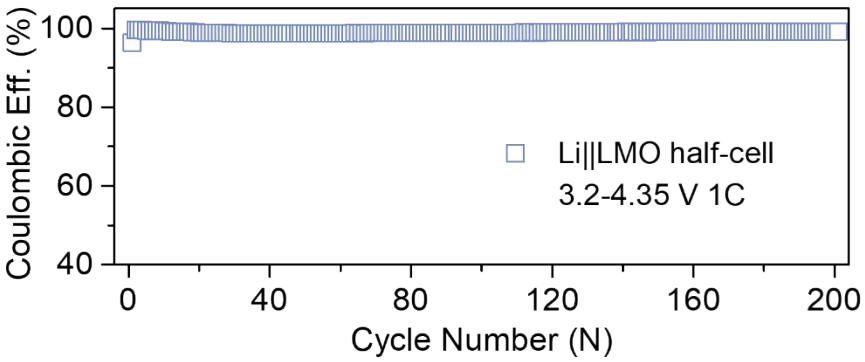

Fig. S3 Cycling performance of Li||LMO half-cell between 3.2 and 4.35 V at 1C.

$$\text{Region I}: LiMn_2O_4\,(\text{cubic}) + Li^+ + e^- \rightarrow Li_2Mn_2O_4\,(\text{tetragonal})$$

$$\text{Region II}: Li_2Mn_2O_4\,(\text{tetragonal}) \rightarrow LiMn_2O_4\,(\text{cubic}) + Li^+ + e^-$$

$$\text{Region III}: LiMn_2O_4\,(\text{cubic}) \rightarrow Li_{1-\delta}Mn_2O_4\,(\text{cubic}) + \delta Li^+ + \delta e^-$$

$$\text{Region IV}: Li_{1-\delta}Mn_2O_4\,(\text{cubic}) + \delta Li^+ + \delta e^- \rightarrow LiMn_2O_4\,(\text{cubic})$$

Fig. S4 The specific reaction equations of four regions in *in-situ* XRD.

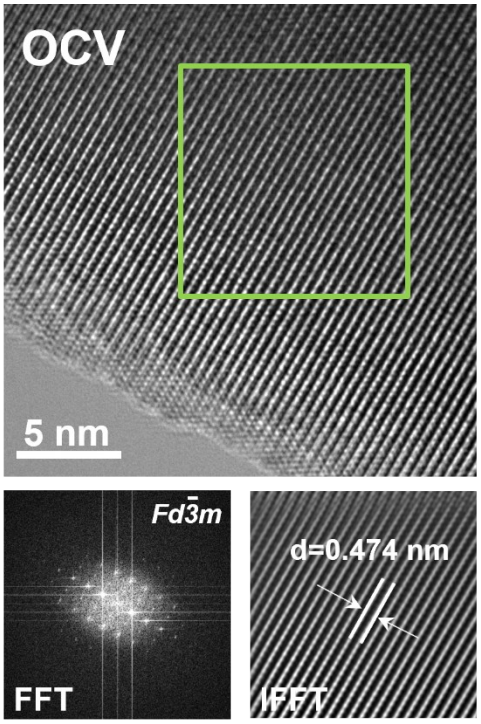

Fig. S5 High-resolution transmission electron microscopy images of the LMO cathode at OCV state. Enlarged images from selected area is shown in insets with its corresponding FFT and IFFT images.

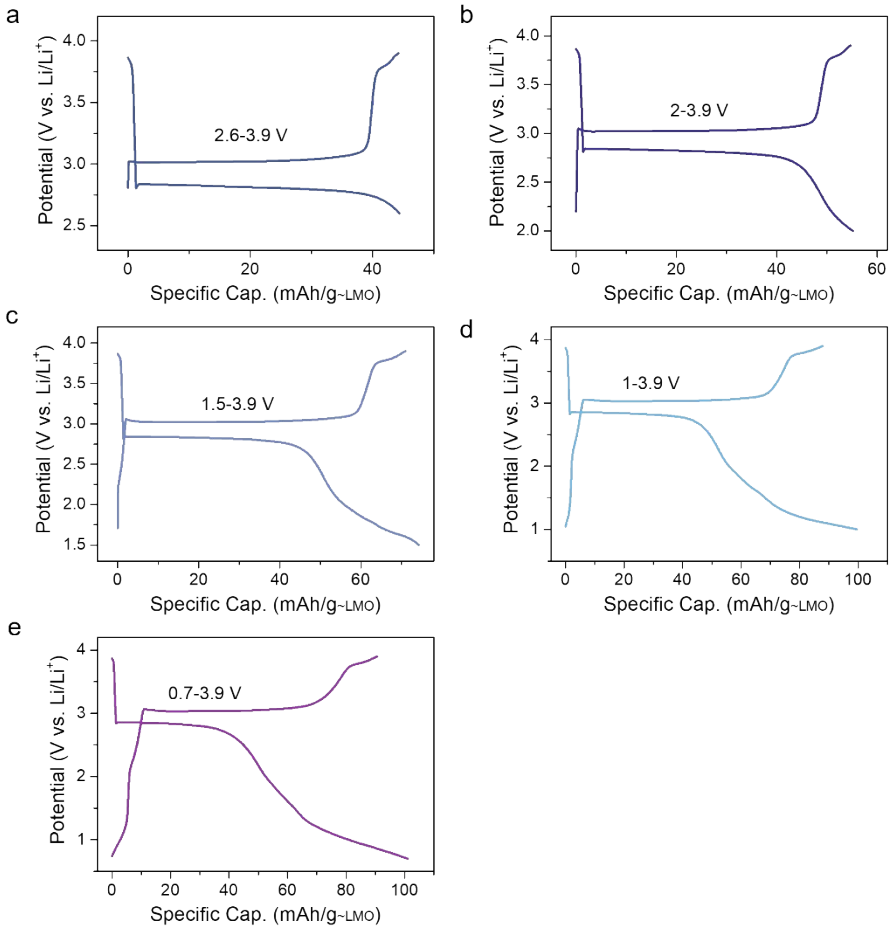

Fig. S6 Voltage profiles of Li||LMO half-cell under different voltage windows of (a) 2.6-3.9 V, (b) 2-3.9 V, (c) 1.5-3.9 V, (d) 1-3.9 V, (e) 0.7-3.9 V. Different specific capacities can be obtained by setting different discharge cut-off potentials. According to the above different voltage profiles with different discharge cut-off potentials, the Coulomb efficiency is close to 100% while the potential is set to 2.6 V or 2 V, suggesting that the additional lithium-ions which are intercalated into the LMO crystal vacancies have no negative on the LMO structure, and thus its structure is reversible. When the discharge cut-off potential is further lowered, the irreversible capacity will appear, indicating that too many additional lithium-ions intercalating into the crystal leads to the collapse of the LMO structure, which is unfavorable for the subsequent cycles of the AF-LMBs. In order to intercalate lithium ions as much as possible, while guaranteeing that the LMO structure would not be damaged so that the structure could be completely reversible, we choose 2 V as the discharge cut-off potential (it could obtain $Li_{1.3}Mn_2O_4$).

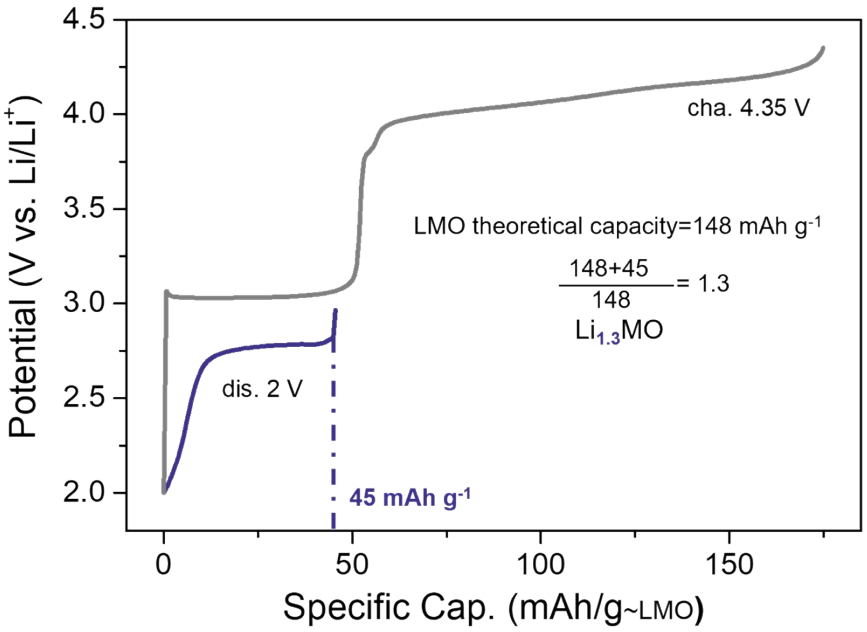

Fig. S7 The charge-discharge curves of Li||LMO half-cell. The first discharge cut-off potential is set to 2 V, following subsequent charge to 4.35 V. When the discharging cut-off potential of Li||LMO half-cell is set to 2 V, by calculating the number of additional lithium-ions which are intercalated into the LMO structure (The detailed calculation process is shown in Fig. S7†), it could obtain $Li_{1.3}Mn_2O_4$ (electrochemical pre-lithiation). The main components of $Li_{1.3}Mn_2O_4$ powder. is shown in Table S2†.

Table S2 Main components of $Li_{1.3}Mn_2O_4$ powder.

Composition	Phases	Space group	Percentage
$Li_{1.3}Mn_2O_4$	$LiMn_2O_4$	*Fd-3m*	70%
	$Li_2Mn_2O_4$	*$I4_1/amd$*	30%

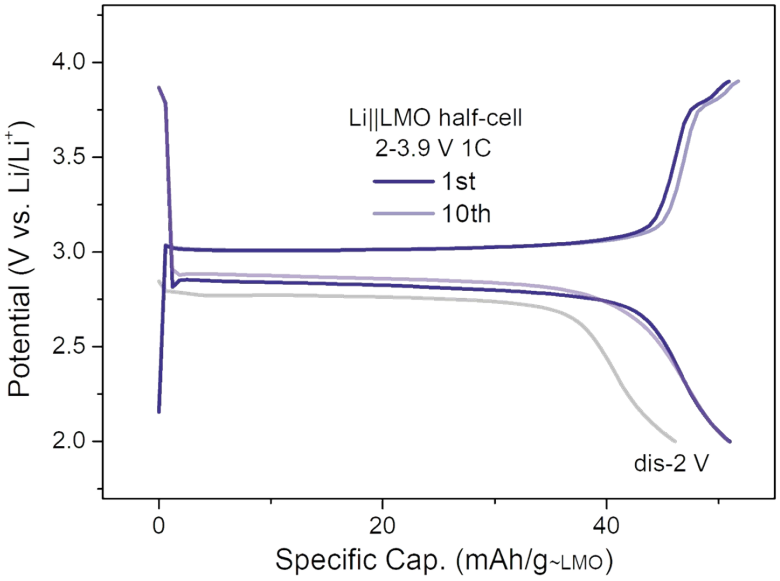

Fig. S8 Voltage profiles of Li||LMO half-cell between 2 V and 3.9 V at 1C. The Coulombic efficiency of the Li||LMO half-cell, which first discharged to 2 V and then cycled under a voltage window of 2-3.9 V, was in close proximity to 100%, indicating that the discharge capacity did not come from electrolyte reduction The x value calculated from the discharge capacity is precisely the amount of additional lithium sources from the anode intercalated into the LMO structure.

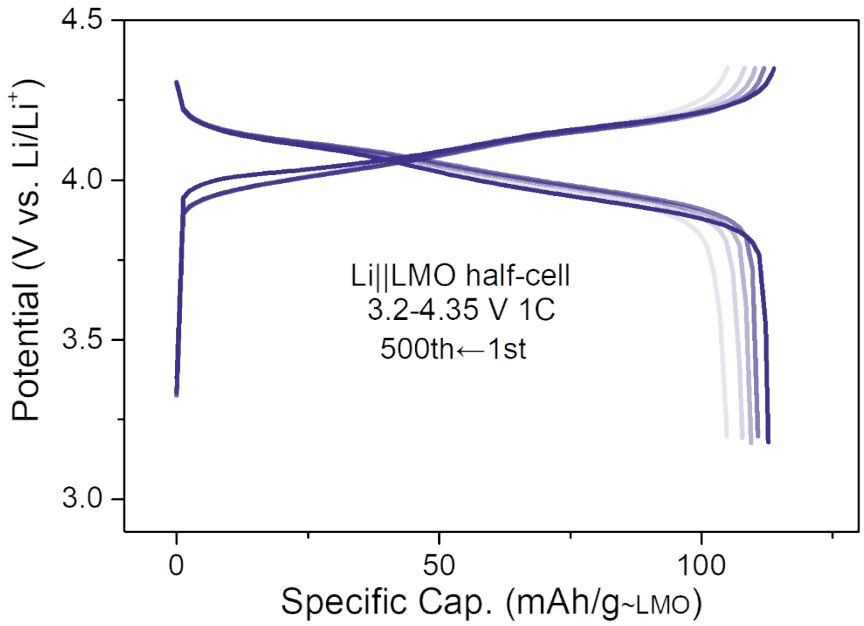

Fig. S9 The charge-discharge curves of Li||LMO half-cell between 3.2 V and 4.35 V for 500 cycles at 1C (denoted as cell-A).

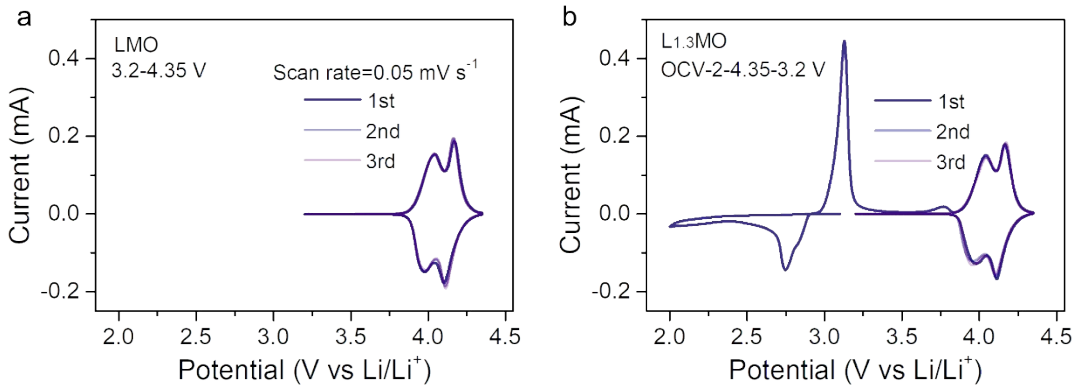

Fig. S10 Cyclic voltammogram (CV) curves of (a) LMO and (b) $L_{1.3}MO$ half-cells in the initial cycles at 0.05 mV s^{-1}.

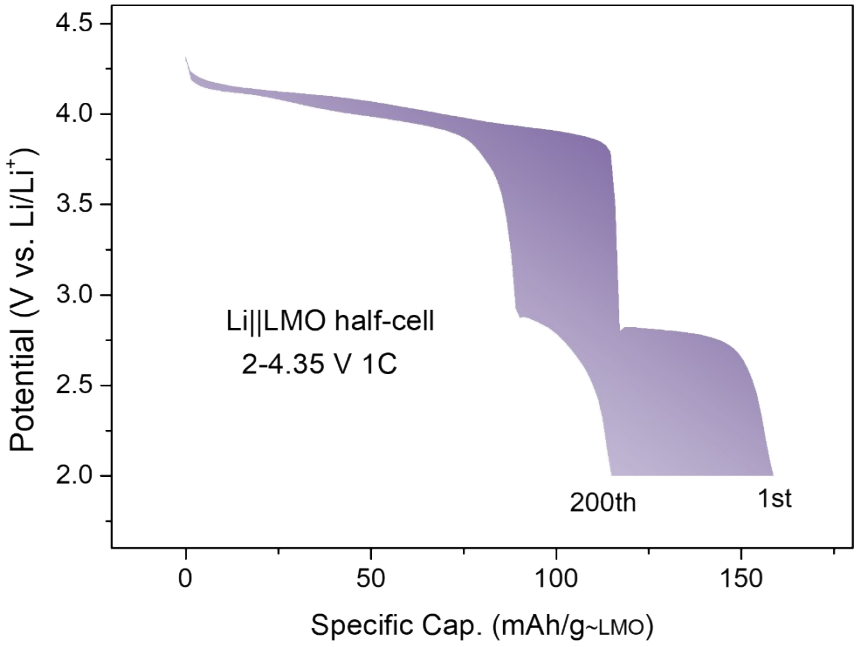

Fig. S11 Voltage profiles of Li||LMO half-cell between 2 V and 4.35 V for 200 cycles at 1C.

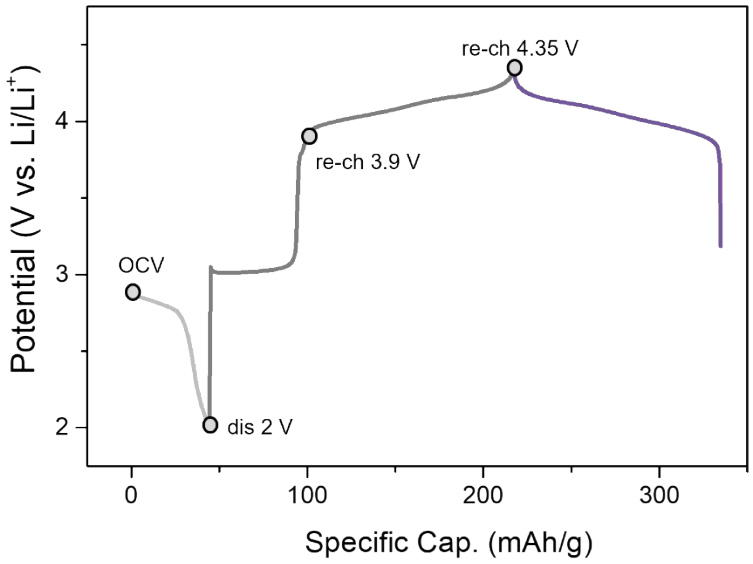

Fig. S12 The corresponding points of the *ex-situ* X-ray absorption structure spectra in Mn K-edge for open circuit voltage (OCV), 2 V discharged, 3.9 V re-charged, and 4.35 V re-charged states are corresponding to the charge-discharge curves of Li||LMO half-cell.

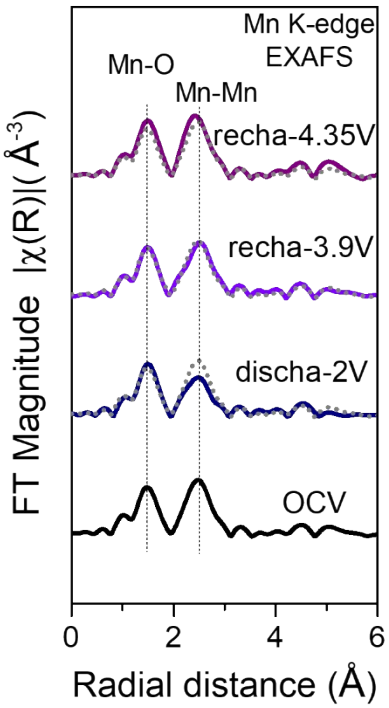

Fig. S13 Extended X-ray absorption fine structure (EXAFS) spectra of the Mn K-edge at different voltage states by contrast with open circuit voltage state.

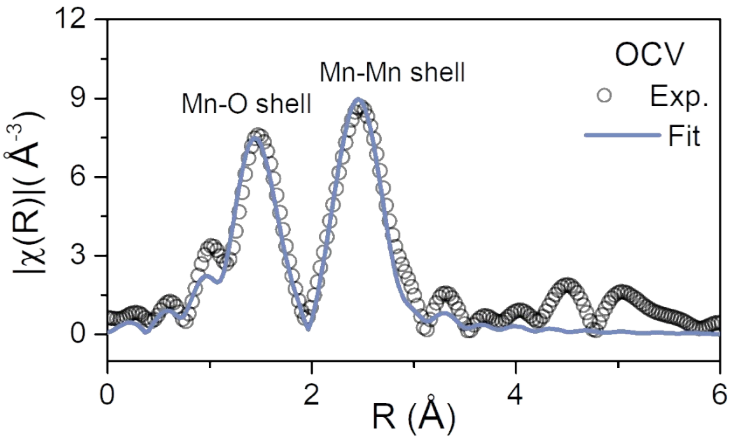

Fig. S14 *Ex-situ* Mn K-edge EXAFS spectra of the LMO sample at OCV state, and the corresponding fitting results.

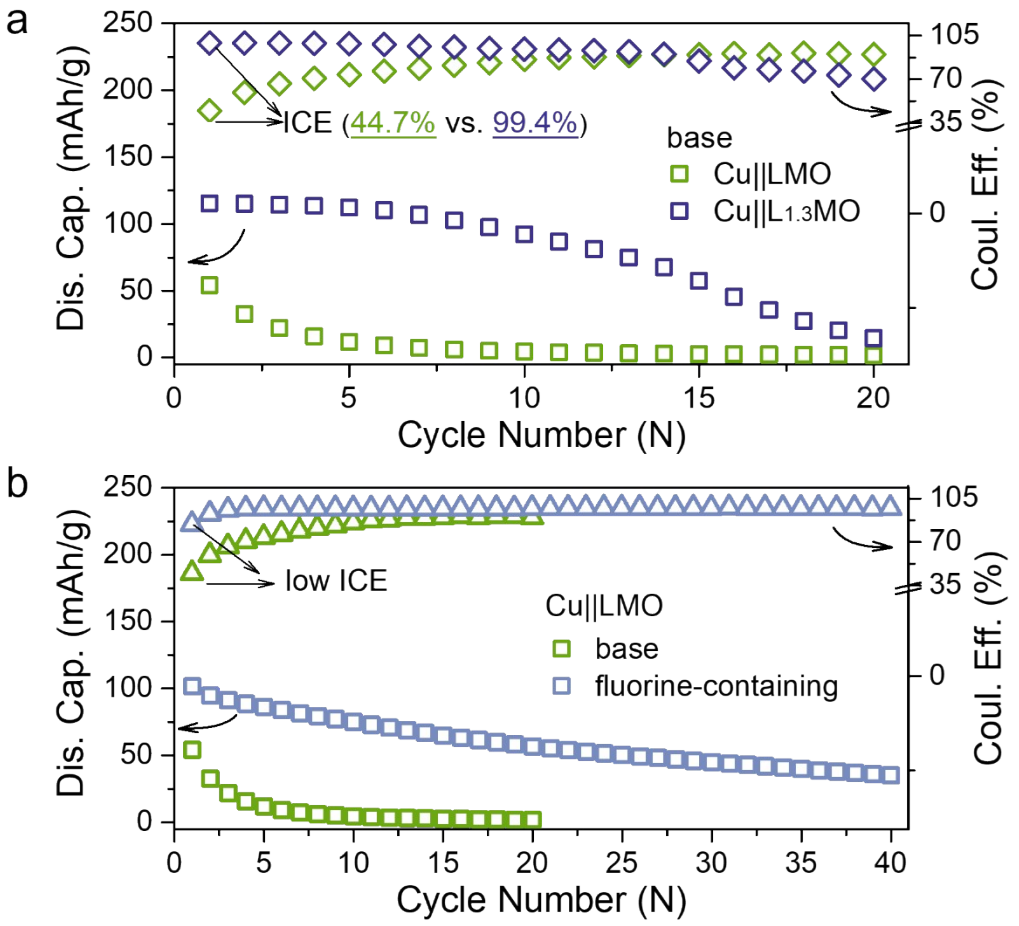

Fig. S15 Cycling performance and CE comparison of (a) Cu||LMO and Cu||$L_{1.3}$MO anode-free coin cell with base electrolyte, (b) Cu||LMO anode-free cion cell with base electrolyte and fluorine-containing electrolyte.

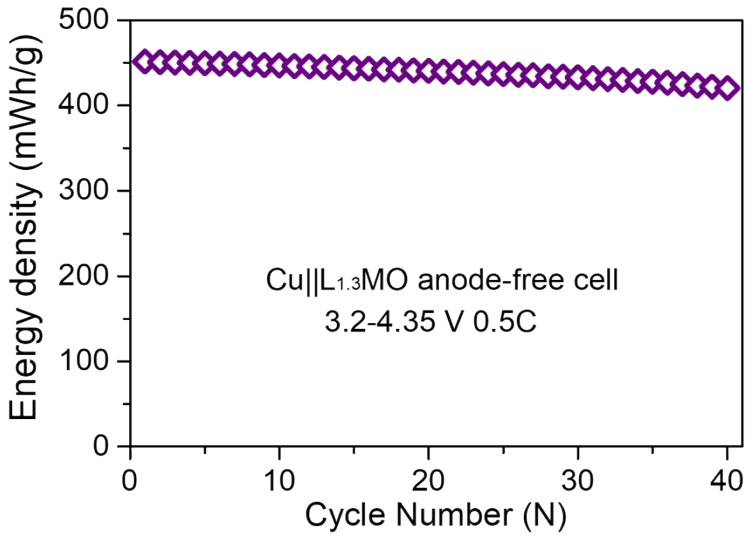

Fig. S16 Energy density of Cu||$L_{1.3}$MO anode-free cell between 3.2 V and 4.35 V for at 0.5C discharge rate.

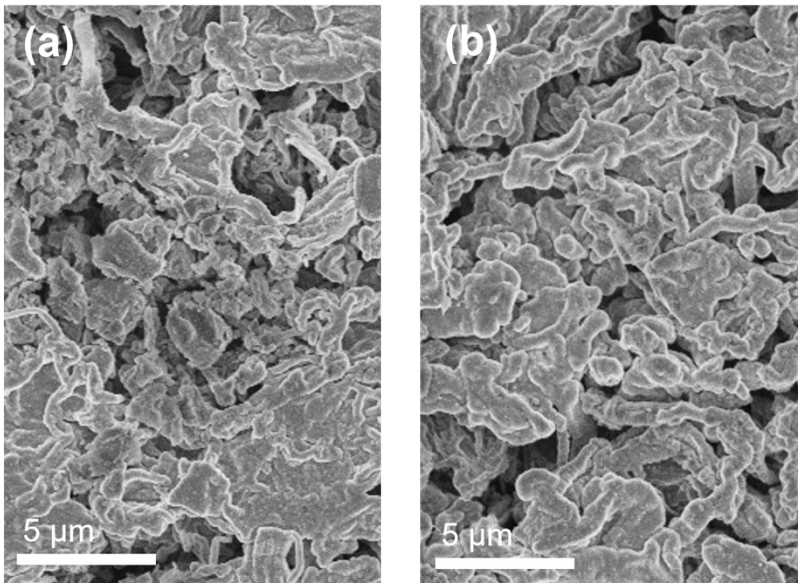

Fig. S17 Surface SEM images of Cu foil in (a) Cu||LMO anode-free cell, (b) Cu||$L_{1.3}$MO anode-free cell after 40 cycles between 3.2 V and 4.35 V at 0.5C discharge rate. From Fig. S17a, vast voids and a number of small debris can be observed on the Cu surface of the Cu||LMO anode-free cell after 40 cycles, which can easily generate "dead Li" during the Li stripping process and facilitate the generation of Li dendrites, resulting in the rapid capacity loss. In contrast, although the Cu surface of the Cu||$L_{1.3}$MO anode-free cell (Fig. S17b) is also partially fragmented, it is much more uniform, which contributes to the electroplating behavior, resulting in showing outstanding capacity retention of 40th with 93.1%

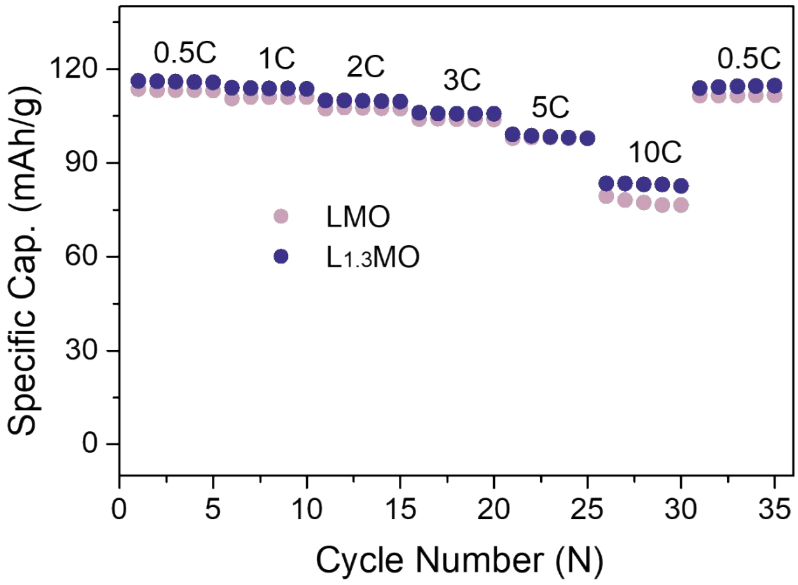

Fig. S18 The rate capabilities of the LMO and $L_{1.3}MO$ cathodes following a rate increase ramp from 0.5C to 10C.

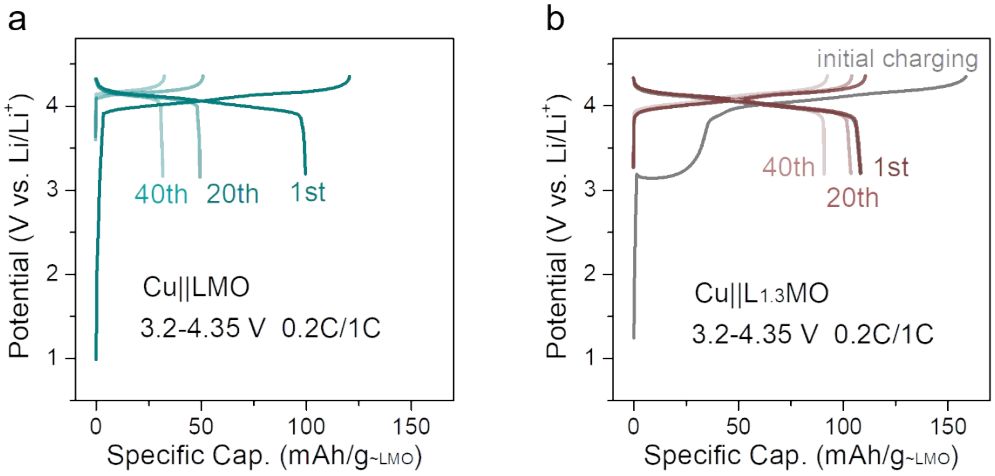

Fig. S19 Charge-discharge curves of (a) Cu||LMO and (b) Cu||$L_{1.3}$MO anode-free coin cell at 0.2C charge and 1C discharge rate.

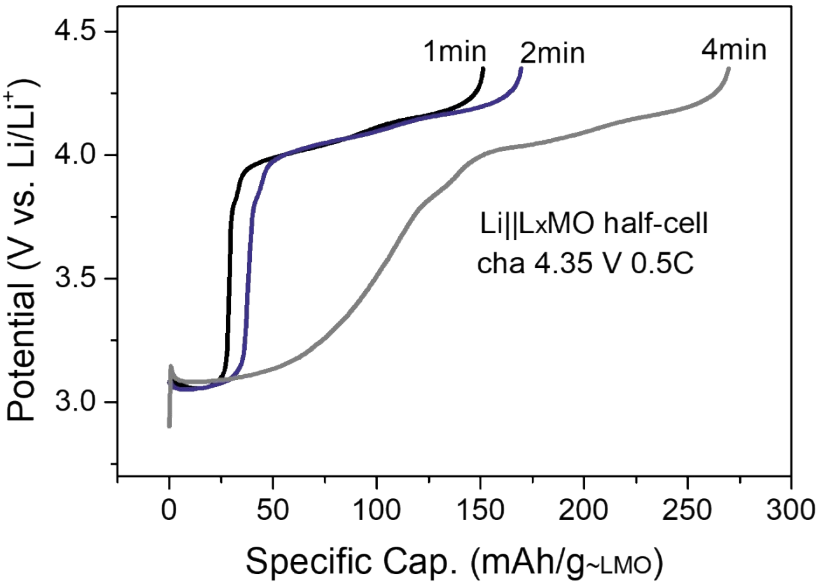

Fig. S20 Voltage profiles of the Li||L_xMO half-cells. The L_xMO ($0 \leq x \leq 2$) cathodes were prepared by contact pre-lithiation method with different contact times. By controlling the contact time, it could regulate precisely the different amounts of lithium-ions intercalating the LMO structure.